Strong disorder leads to scale invariance in complex biological systems

Stella Stylianidou, Thomas J. Lampo, Andrew J. Spakowitz, and Paul A. Wiggins

Strong disorder leads to scale-invariance in complex biological systems

Stella Stylianidou,[1] Thomas J. Lampo,[2] Andrew J. Spakowitz,[2] and Paul A. Wiggins[1]

[1]*Departments Physics, Bioengineering and Microbiology, University of Washington, Seattle, WA, 98195*
[2]*Department of Chemical Engineering, Applied Physics,*
Materials Science and Biophysics Program, Stanford University

Despite the innate complexity of the cell, emergent scale-invariant behavior is observed in many biological systems. We investigate one example of this phenomenon: the dynamics of large complexes in the bacterial cytoplasm. The observed dynamics of these complexes is scale-invariant in three measures of dynamics: mean-squared displacement (MSD), velocity autocorrelation function and the step-size distribution. To investigate the physical mechanism for this emergent scale-invariance, we explore minimal models in which mobility is modeled as diffusion on a rough free energy landscape in one dimension. We discover that all three scale-invariant characteristics emerge generically in the strong disorder limit. (Strong disorder is defined by the divergence of the ensemble-averaged hop time between lattice sites.) In particular, we demonstrate how the scale-invariance of the relative step-size distribution can be understood from the perspective of extreme-value theory in statistics (EVT). We show that the Gumbel scale-parameter is simply related to the MSD scaling parameter. The EVT mechanism of scale-invariance is expected to be generic to strongly-disordered systems and therefore a powerful tool for the analysis of other systems in biology and beyond.

I. INTRODUCTION

Although most biological phenomena have well-defined and characteristic time and length scales, there are intriguing examples of emergent scale-invariant behavior which are self-similar over a wide range of scales [1–3]. In the context of random motion, diffusion is the canonical scale-invariant effective model, but our experimental observations argue for the existence of other generic scale-invariant effective models describing random motion [4]. In this paper, we propose a natural mechanism for the emergence of non-diffusive but scale-invariant behavior which can be understood from the perspective of the statistical properties of the extreme values of random variables [5, 6]. Extreme Value Theory (EVT) has already been used in many interesting contexts (*e.g.* [7–12]) and our results suggest that this approach may be a powerful tool for understanding dynamics in the cell.

The movement of large complexes in the bacterial cytoplasm is an example of a biological system with emergent scale-invariance [4]. Our laboratory and others have previously characterized the dynamics of large exogenous complexes by tracking the motion of mRNA molecules bound by the fluorescent fusion MS2-GFP which forms complexes comparable in size to the ribosome [4, 13–18]. In the following discussion we shall refer to these molecular complexes as *particles*. To avoid the complications introduced by the tighter confinement of the particle along the short axis of the rod-shaped bacterium, we shall focus on the one-dimensional motion of the particle along the long axis of the cell. As we have previously discussed [4], the observed particle motion is scale invariant from the perspective of three distinct metrics: (i) mean-squared-displacement analysis (MSD), (ii) the step-size distribution and (iii) the velocity autocorrelation function.

A. Existing models

Four mechanisms are commonly invoked to model sub-diffusive phenomena: Continuous Time Random Walk (CTRW), fractional Brownian motion (fBm), inhomogeneous media (*e.g.* spatial dependence of the diffusion coefficient) and scaled-Brownian motion (time-dependent diffusivity) [19, 20]. In each of these models, there is a memory mechanism that results in non-diffusive motion. In a CTRW, particles execute stochastic hops after a randomly-distributed wait time. Power-law-distributed wait times lead to sub-diffusive motion. In the closely related inhomogeneous media model (patch model), particles diffuse through quenched patches (*i.e.* static) with patch-specific diffusion coefficients. For strong enough disorder, these models result in sub-diffusive motion [21, 22]. (Both CTRW and inhomogeneous media are closely related to the trap model that we will discuss shortly.) In scaled-Brownian Motion, the diffusion coefficient evolves in time [20]. Finally, fractional Brownian motion (fBm) is a process closely related to Brownian motion except that that the motion increments (steps) are not independent but power-law correlated [19, 20].

None of these mechanisms predict the observed phenomenology without add mechanisms [4]. For instance, of these models only fBm describes the observed anti-correlation between successive steps in the motion [4]. But, the steps in an fBm are Gaussian distributed, in contrast with the Laplace-distributed steps of the observed dynamics. One practical approach to constructing a model with all the desired properties is to combine the fBm model with one of the mechanisms for generating a non-gaussian steps-size distribution. For instance, Granick and coworkers have proposed a model in which the diffusion coefficient is exponentially-distributed and quenched (Exp-D) to generate Laplace-distributed steps

[23]. We have recently proposed combining the fBm and Exp-D models (fBm-Exp-D) to describe the observed dynamics [4]. Although this model can fit most of the observed phenomenology [4], it is essentially an empirical model where both the distribution of diffusion coefficients as well as the fBm Hurst parameter are fit to the data, but the model gives no insight into either the source of the distribution of diffusion coefficients nor the mechanisms that give rise to fBm. A more satisfactory model would demonstrate how these scale-invariant characteristics are a generic emergent property of the complex systems. In this paper, we will explore a family of models where the observed phenomena arise generically in the strong disorder limit.

The paper is organized as follows: In Sec. II, we briefly describe the experimental methods used to capture the trajectory data. (We will present one new experimental result in the analysis in Sec. IV F.) In Sec. III, we define the models for particle mobility. In Sec. IV, we characterize the models using numerical simulations. We describe how strong disorder in a barrier model appears to generically generate the observed scale-independent motion we observe. In Sec. V, we describe an analytic framework for understanding the strong disorder limit.

II. EXPERIMENTAL METHODS

We use the MS2-mRNA system as a probe for the dynamics of large complexes in the cytoplasm. The system (from I. Golding) consists of the *E. coli* strain DH5α-Z1 carrying two plasmids, the first encoding the GFP-MS2 protein fusion for labeling the mRNA and the second low copy plasmid carry an inducible message with a 96-tandem repeat of MS2 binding sequences [14].

A detailed experimental and imaging protocol is given in Ref. [18]. In short, the cells were grown overnight in Luria Broth media (LB) with the appropriate antibiotics, diluted and grown to approximately mid-log phase. The cells were then induced with IPTG (Isopropyl b-D-1-thiogalactopyranoside 1 μM) and aTc (anhydrotetracycline 10 ng/mL) for 15 min at 30°C. A 2 mL innoculum of cell culture was spotted onto agarose-media pads (2% Invitrogen UltraPure™ LMP Agarose REF: 16520-050) and sealed with VaLP (1:1:1 vaseline:lanolin:paraffin). Time-lapse phase-contrast and wide-field-fluorescence microscopy images were collected at 1 second and 1 minute time intervals and trajectory data were analyzed using the custom made MATLAB software (The MathWorks, Natick, MA) SuperSegger [24]. For the 1-minute-time-interval data, only full-cell-cycle cells were used for the analysis.

III. MODEL

The bacterial cytoplasm is an extremely crowded and non-equilibrium environment [25] and it has recently
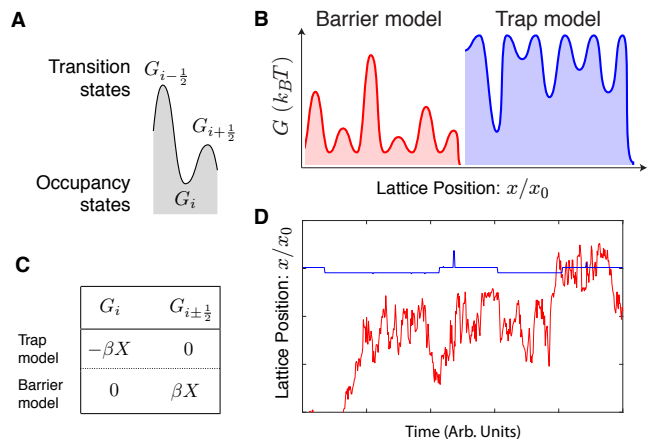

FIG. 1. **Panel A:** The dynamics is modeled as transitions between adjacent occupancy states (integer sites) through transitions states (half-integer sites). **Panel B and C:** To understand the generic model, we study two limiting cases: the trap and barrier models. In the trap model, the occupancy states have free energies $-\beta X$ where X is distributed like a one-dimensional chi-squared random variable and β is a parameter controlling the disorder strength. In the barrier model, the transition states have free energies βX. **Panel D:** A representative trajectory from each model is shown. The trap and barrier models have qualitatively different dynamics. The trap model shows persistent pausing behavior in the motion corresponding to long-lived trapping events. The barrier model shows a reflection behavior caused by large energy barriers. (Simulation details are described in Sec. D 1.)

been proposed that it behaves like a glass [26]. Due to the strong crowding in the cell, it seems natural to investigate random walks in a disordered free-energy landscape [19]. We model the cytoplasm as a one-dimensional lattice. We represent integer sites in the lattice as occupancy states and half-integer sites as transition states. (See Fig. 1A.) The free energy (in units of $k_B T$) of each state is G_i. The hopping rate k and average hopping time τ from site i to sites $i \pm 1$ have the Arrhenius dependence:

$$k_{i \to i\pm 1} = \tau^{-1} = t_0^{-1} \exp(G_i - G_{i\pm\frac{1}{2}}), \qquad (1)$$

where t_0 represents a fundamental relaxation time in the system and the free energy difference in the exponent represents the height of the free energy barrier to transition through the transition state. It is important to stress that the free energies are effective quantities defined by the transition rates.

We will treat the free energies as *quenched disorder*: The free energies are static in time for each lattice site. In reality, the disorder is dynamic, but this approximation is motivated by the assumption that there are barriers whose dynamics are slower than the dynamics of interest (In fact, this assumption has significant experimental support. We have explicitly investigated the dynamics of nearly all non-diffuse proteins in *E. coli* and

shown that there is structural disorder that persists on times scales comparable to the cell cycle [27].) In the most general model, the free energies of both the occupancy and transition states are represented as random variables [19]. But, it is useful to consider two limiting cases: In the *trap model*, the depth of the transition state is stochastic whereas the free energies of all transition states are 0. In the *barrier model*, the free energies of the barriers are stochastic whereas the free energies of the occupancy states are 0 (Fig. 1C). These models were originally studied in the context of electron transport in the 1980s [19, 28, 29] and it is already well known that strong disorder, defined by the divergence of the disorder-averaged hopping time:

$$\langle \tau \rangle_G \to \infty, \tag{2}$$

results in sub-diffusion [19]. It is necessary to choose a semi-infinite interval distribution for the free energy so that the traps and barriers preserve their nature ($G_{i\pm\frac{1}{2}} > G_i$) and to achieve the strong disorder limit. A canonical distribution with these properties is the one-dimensional chi-squared distribution, multiplied by a unitless disorder strength β. As we will show, the explicit functional form of the free energy distribution will not be of central importance. It is straight-forward to show that in the chi-squared disorder model, $\beta \geq \frac{1}{2}$ satisfies the definition of strong disorder (Eqn. 2).

IV. SIMULATED RESULTS

We begin our investigation with a numerical experiment: We simulate particle dynamics in the trap and barrier models. (A detailed description of the simulations can be found in the appendix, Sec. B.) We compare the simulated characteristics of the motion to the experimental characteristics we have previously described in detail [4, 18].

A. Disorder strength determines MSD scaling

A common metric for the analysis of particle trajectories is the Mean Squared Displacement (MSD), which takes the form of a power law for scale-invariant systems:

$$\left\langle \left[\Delta x^2(t)\right]_{t=0} \right\rangle_G \approx 2\, D\, \delta t^\alpha, \tag{3}$$

which we will call E-MSD for ensemble-averaged MSD where the angle brackets represent an ensemble average, $\Delta x(t) \equiv x(t+\delta t) - x(t)$ is the displacement over lag time δt with start time t, α is the scaling exponent and D is a generalized diffusion coefficient. The motion is characterized by the scaling exponent α: If $\alpha = 1$, the motion is diffusive and $\alpha < 1$ corresponds to sub-diffusive motion.
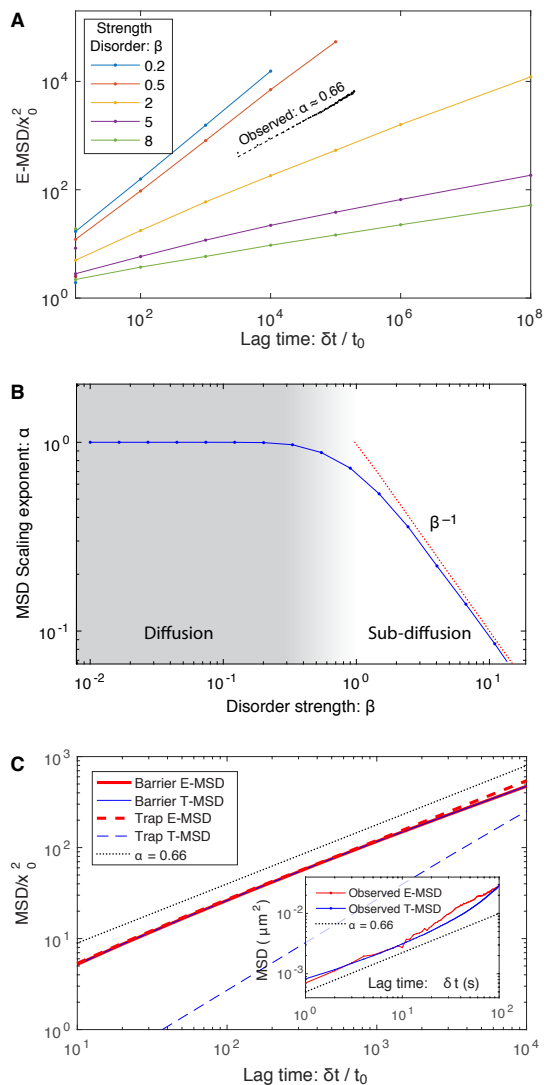
FIG. 2. **Panel A: Disorder strength controls mobility.** Simulated MSD curves for a range of disorder strength β as a function of lag time δt. (Simulation details are described in Sec. D 2.) **Panel B:** MSD scaling coefficient α versus disorder strength β. The dynamics in the barrier model were diffusive ($\alpha = 1$) for $\beta < \frac{1}{2}$ and sub-diffusive for $\beta > \frac{1}{2}$. The disorder strength is $\alpha \approx \beta^{-1}$ in the strong disorder limit. (Simulation details are described in Sec. D 3.) **Panel C: Ergodicity.** Simulations suggest that the barrier model is ergodic: E-MSD and T-MSD are equal. The trap model is non-ergodic: There is a large mismatch between E-MSD and T-MSD due to aging phenomena. (Simulation details are described in Sec. D 4.)

To understand the relation between disorder strength and the dynamics, we compute the MSD for different disorder strengths in both the barrier and trap models. (See Fig. 2 for simulations of the barrier model. Simulations of trap model are analogous but not shown.) As the roughness of the free energy landscape increases, we expect the motion to slow down and result in a reduction in the MSD. This reduction could be realized via
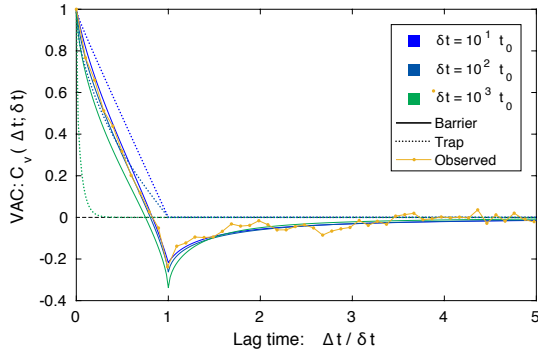
FIG. 3. **Velocity autocorrelation function (VAC) for trap and barrier model.** The velocity autocorrelation function $C_v(\Delta t; \delta t)$ is shown for the trap and barrier model for strong disorder, where Δt is the delay time and δt is the lag time over which the displacements are calculated. The barrier model shows excellent qualitative and quantitative agreement with experimental observations ($\delta t = 10$ s). The trap has no anti-correlation between successive steps, and therefore is inconsistent with observations. (Simulation details are described in Sec. D 5.)

two distinct changes in the MSD: A reduction in the effective diffusion coefficient D or the scaling exponent α. For weak disorder $\beta < \frac{1}{2}$, only the effective diffusion coefficient D decreases with increasing disorder strength β and the scaling exponent $\alpha = 1$ is diffusive at long times [30]. But, for strong disorder, $\beta > \frac{1}{2}$, the scaling exponent α decreases with increasing β. Simulation suggests a simple approximate relation between disorder strength and the scaling exponent in the strong-disorder limit: $\alpha \approx \beta^{-1}$. (See Fig. 2B.) In conclusion, both the trap and the barrier model can match the observed sub-diffusive MSD.

B. Ergodicity

Another key characteristic of sub-diffusive motion is ergodicity: the equivalence of temporal and ensemble averaging. The failure of these two averages to be equivalent is typically interpreted to reveal an aging phenomena [19]. To probe the ergodicity we compare an ensemble-averaged MSD (Eqn. 3) to the time time-averaged MSD (T-MSD):

$$\langle \Delta x^2(t) \rangle_{t,G}, \tag{4}$$

which are averaged over both the start time as well as ensembles.

As we have previously discussed [4], the experimental data reveals little ergodicity breaking on short times scales and some on timescales comparable to the cell cycle which is consistent with the large-scale cellular changes that occur on these time-scales. (See the inset in Fig. 2C) To test the trap and barrier models, we computed both the ensemble and time-averaged MSDs in
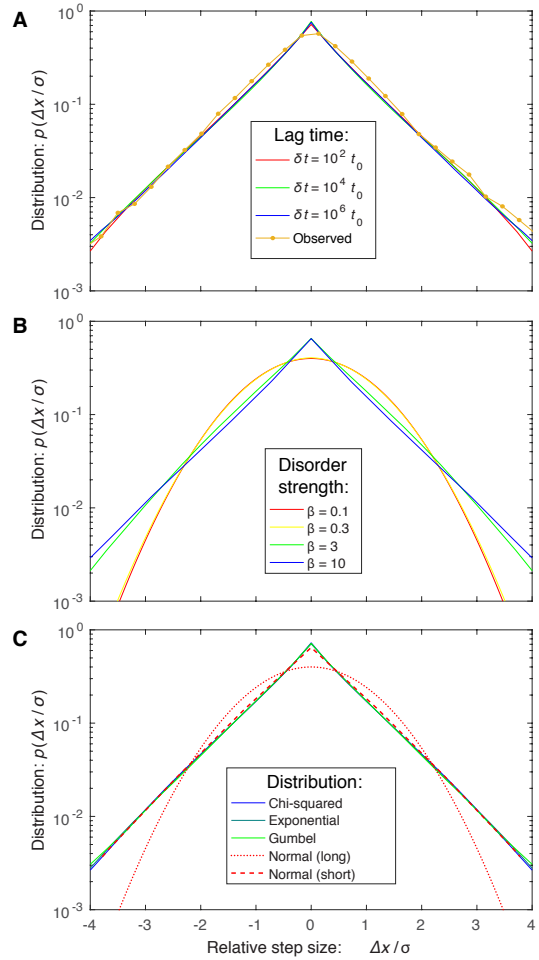

FIG. 4. **Panel A:** The distribution of relative step sizes is approximately scale-invariant in the strong disorder limit. The simulated distribution function for the barrier model is shown for lag times varying over four orders of magnitude. All distribution functions are Laplace-like in agreement with the experimental data ($\delta t = 10$ s). (Simulation details are described in Sec. D 6.) **Panel B:** Strong disorder ($\beta > \frac{1}{2}$) leads to Laplace-like distributions while weak disorder ($\beta < \frac{1}{2}$) results is Gaussian-like step-size distributions. (Simulation details are described in Sec. D 7.) **Panel C:** In the strong disorder limit, the relative step-size distribution is insensitive to the distribution of the random free energies G, which is demonstrated by the first three disorder models: Chi-squared, Exponential and Gumbel. For weak disorder (Normal model), Laplace-like distributions can still be observed at short lag times (red dots) but at long times, the distribution approaches Gaussian (red dashed). (Simulation details are described in Sec. D 8.)

the two models. Simulations reveal strong ergodicity breaking in the trap model and no ergodicity breaking in the barrier model. (See Fig. 2C.) The mechanism of ergodicity breaking (*i.e. aging*) in the trap model is already well known in the context of the closely related CTRW [19]: Over time, the number of trapped particles grows, leading to a reduction in the average mobility. Although ergodicity breaking is observed in experiment, it is not

significant at short times, in contrast to the predictions of the trap model. Therefore the observed absence of ergodicity breaking at short times is consistent with the barrier model but not the trap model.

C. Anti-correlated motion

Although both trap and barrier models are sub-diffusive, the trajectories shown in Fig. 1D are clearly distinct at a qualitative level. The trap model shows characteristic long-lived pausing events which were qualitatively absent in the observed traces. (Experimental trajectories are shown in Ref. [18].) In contrast, the presence of barriers has a much more subtle effect on the motion. Barriers lead to the reflection of the particles but stochastic changes in direction are present in canonical Brownian motion, making the reflection phenomenon difficult to distinguish from regular brownian motion by inspection. We find that the reflection phenomenon *does* lead to a clear statistical signature: negative velocity autocorrelation, as discussed below.

A canonical method to characterize the memory is computing the correlation between steps using the velocity autocorrelation function (VAC–*i.e.* a displacement correlator):

$$C_v(\Delta t; \delta t) \equiv \langle \Delta x(t)\, \Delta x(t+\Delta t) \rangle_G \, / \, \langle\, \Delta x(t)\, \rangle_G^2, \quad (5)$$

where Δx is the displacement over lag time δt and the expectation is over multiple ensembles of disorder (G). As we have previously reported, the observed velocity-autocorrelation function $C_v(\Delta t; \delta t)$ is negative for $\Delta t > \delta t$ and roughly scale invariant [4]. (See Fig. 3.)

To test the barrier and trap models, we simulated the VAC in the two models. The predictions of the trap model do not match experiment: The VAC is 0 for $\Delta t > \delta t$. On the other hand, the barrier model predictions are in excellent quantitative agreement with experiment. (See Fig. 3.) The VAC is both negative and scale invariant (depends only on $\Delta t/\delta t$) and has no additional fitting parameters since the disorder strength β is determined from fitting the MSD. The simulations clearly support the barrier and are inconsistent with the trap model.

The observation of a negative velocity-autocorrelation function is often interpreted to imply that the medium is viscoelastic [16], but this is an emergent rather than a microscopic characteristic of the barrier model. The agreement between the observed and predicted velocity autocorrelation process is unremarkable from another perspective: For stationary processes, the velocity autocorrelation function is half the second derivative of the MSD. In the context of strong disorder, the trap model is non-stationary and therefore their velocity autocorrelation function and MSD are *not* equivalent. For this reason, it is essential to measure and analyze both the MSD and the VAC independently [4, 16].

D. Step sizes are Laplace distributed for strong disorder

The last striking scale-invariant feature of the motion is the relative step-size distribution [4]:

$$\overline{p}(\Delta x/\sigma; \delta t) \equiv \langle p(\Delta x/\sigma; \delta t) \rangle_G, \quad (6)$$

measured by histogramming step sizes from multiple trajectories and computed by averaging over the ensemble. To test the barrier model, simulated the disorder-averaged step-size distribution. In the strong disorder limit $\left(\beta > \frac{1}{2}\right)$, we discovered that the step-size distribution is Laplace-like and scale invariant (Fig. 4AB), qualitatively matching the observed distribution. Since the choice of the chi-squared distribution was motivated by convenience not physics, the agreement between the model and observations suggest that the Laplace-like step-size distribution must be universal. To investigate this hypothesis, we simulated a number of other distributions: exponential, normal and Gumbel. In all cases, strong disorder resulted in step-size distributions which are Laplace-like, whereas weak disorder results in Gaussian-like distributions in the long time limit (Fig. 4C). These simulations suggest a Renormalization-Group behavior: The functional form of the macroscopic step-size distribution is insensitive to the underlying microscopic distribution of the free energy barriers. In summary, the barrier model naturally reproduces the step size distribution in the strong disorder limit without the need to tune the distribution of barrier free energies.

E. Testing the quenched diffusion constant model

We have previously proposed that the mechanism that gives rise to the observed Laplace distribution is an exponential distribution of quenched diffusion coefficients. This model predicts that the distribution of step sizes within a single trajectory is Gaussian. The Laplace distribution arises from pooling the data from multiple trajectory with exponentially distributed quenched diffusion coefficients. Unfortunately the step-size histograms for individual trajectories are not well sampled, but it is straightforward to analyze this question statistically. Consider two competing models for the stepping process: (i) Steps are Gaussian distributed around 0 with a trajectory-specific variance σ_I^2 versus (ii) Steps are Laplace distributed with an trajectory-specific decay rate λ_I. To measure the relative statistical support for the two models we use information-based inference [31, 32]: We compute the Akaike Information Criterion (AIC) for the two models. The model with the smallest AIC value is selected. (The expression for AIC in the respective models has a simple analytic form that can be written in terms of empirical expectations over moments of the observed steps, as shown in Appendix
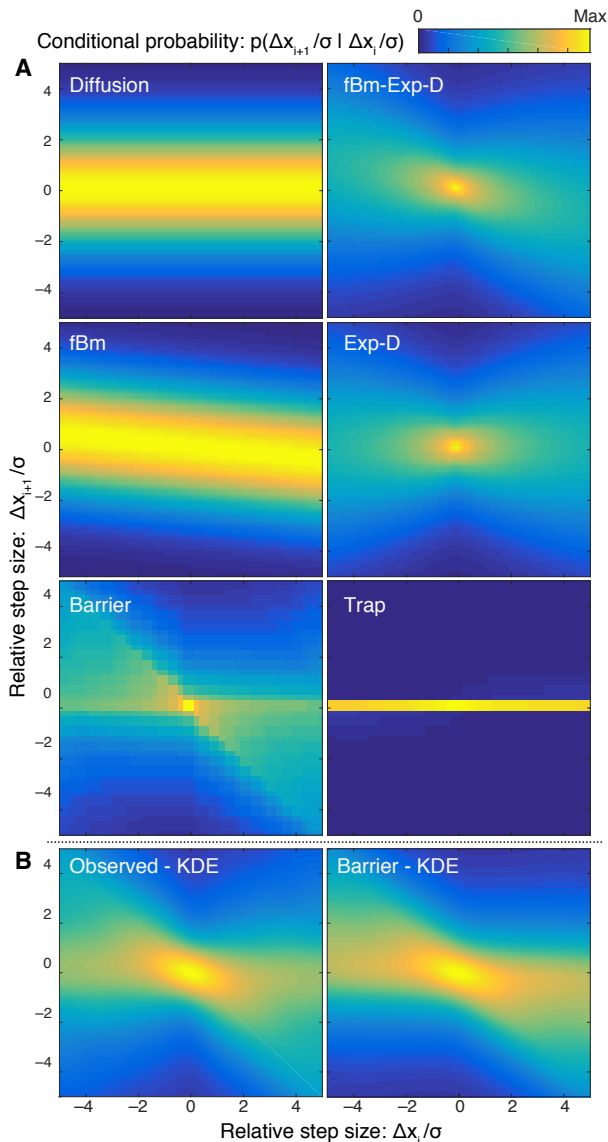
FIG. 5. **Analyzing the step size memory. Panel A:** The conditional probability distribution for relative step size: $p(\Delta x_{i+1}/\sigma|\Delta x_i/\sigma)$ simulated in competing models for particle mobility. The structure of the distribution reveals qualitative difference betweens the models. (Simulation details are described in Sec. D 9.) **Panel B:** Kernel Density Estimate (KDE) of the observed conditional probability distribution compared to the barrier model KDE. Experimental data ($\delta t = 1$ min) of mRNA-MS2 molecular complexes (sample size: $N = 2.5 \times 10^5$). (Simulation details are described in Sec. D 10.)

Sec. A 1.) The difference in the information criteria is:

$$\text{AIC}_{(i)} - \text{AIC}_{(ii)} = 1.8 \times 10^3 \text{ nats}, \tag{7}$$

strongly favoring the Laplace over the Gaussian distributed model. (The relative statistical weight, the Akaike weight, is the exponential of ΔAIC [31, 32].)

Since a trajectory-specific diffusion coefficient is not required to generate Laplace-distributed steps in the

barrier model, it is therefore informative to test whether the data supports trajectory-specific models a single model describing all steps. Again, we can compute the difference in AIC for a (iii) single decay constant model versus (ii) a trajectory-specific decay constant model:

$$\text{AIC}_{(iii)} - \text{AIC}_{(ii)} = 3.4 \times 10^4 \text{ nats}, \tag{8}$$

strongly favoring the trajectory specific-decay-constant model. This evidence suggests that there is potentially particle-to-particle or cell-to-cell variation, a conclusion that is not surprising in a biological context.

F. Conditional probability and memory

The form of the MSD, VAC and step-size distribution were all known prior to our proposing the barrier model to describe the mobility. We wished to predict the dependence of an uncharacterized metric of motion to test the barrier model. The velocity-autocorrelation function can be understood as a moment of the conditional probability distribution for step-size: $p[\Delta x(t + \delta t)|\Delta x(t)]$ which provides a more informative test than the velocity autocorrelation function alone. Furthermore, the models make qualitatively different predictions for the distribution, as is shown in Fig. 5A. Since competing models make qualitatively different predictions for the structure of the conditional probability, we believe this distribution is a powerful tool for distinguishing between models of the dynamics.

To test our model, we computed the Kernel-Density-Estimate (KDE) of the conditional probability distribution for step-size and compared it to the models. Both the barrier and fBM-Exp-D model [4] provides excellent qualitative agreement with the observed distribution (Fig. 5B). In both the observed data and the model, there is a strong diagonal band which represents the characteristic anti-correlation between subsequent steps.

G. Mechanism for sub-diffusion

To understand the mechanism for sub-diffusion, it is informative to compute the Green's function $p[x(t + \delta t)|x(t)]$ *without* averaging over disorder. (See Fig. 6.) The characteristic feature of the Green's function is the block-diagonal structure which is the consequence of the largest stochastic barriers. The physical mechanism for this structure can be understood intuitively: In the strong disorder limit, particles rapidly jump over barriers with hop times τ less than the lag time δt, but the particle motion is limited by the presence of barriers where the hop time is much longer than the lag time ($\tau \gg \delta t$). The uniformity of the probability density in the blocks demonstrates that the motion is limited by these large barriers for strong disorder ($\beta \gg \frac{1}{2}$).

Qualitatively, the motion can be understood as follows: As the time-scale increases, the free energy of the
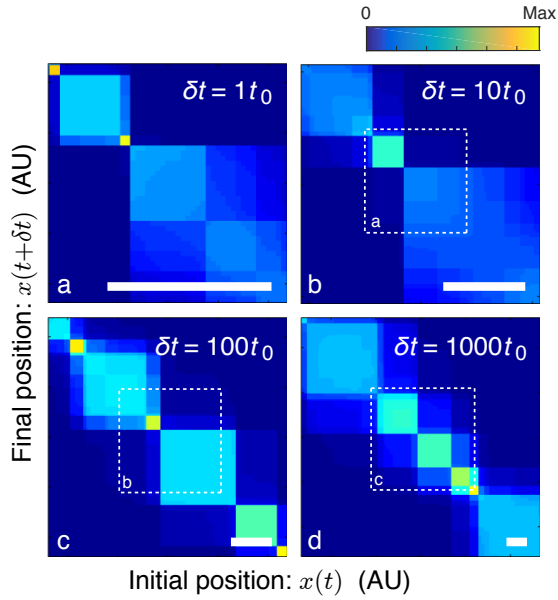
FIG. 6. **Self-similarity of the Green's function with fixed disorder.** The heat maps represent the Green's function $p[x(t + \delta t)|x(t)]$ for $\beta = 5$ for lag times spanning four orders of magnitude. To illustrate the stochastic self-similarity, the position x is rescaled (zoomed-out) with increasing lag time to keep the MSD fixed. (The length of the white scale bar is fixed in unscaled units.) The stochastic block-diagonal structure of the Green's function is scale-free. The block-diagonal form implies the motion is limited by the slowest step on all scales. (Simulation details are described in Sec. D 11.)

largest barrier that can be jump increases logarithmically. Displacement and free energy have an analogous relation: The largest free energy encountered grows logarithmically with displacement.

H. Mobility in Dim > 1

So far, we have worked in one spatial dimension, along the long axis of the cell, to avoid consideration of the confinement along the short axis. An important consideration is to consider how our results generalize to three dimensions. The dynamics of random uncorrelated barrier models changes fundamentally in the long-lag-time limit in larger dimension: No matter how strong the disorder, large barriers can be avoided by traveling a circuitous path. Barrier models are therefore always diffusive at *sufficiently* long times in dimension greater than one [33]. These models are qualitatively similar to obstructed diffusion (obstacles, Lorentz-like and fence models [34]). However, we hypothesized that dynamics observed in one dimension might still be applicable for finite lag times, which is supported by simulation. (See Fig. 7.) In practice, the crossover between sub-diffusive dynamics and diffusion may be extremely long. On shorter times, the qualitative effect of the
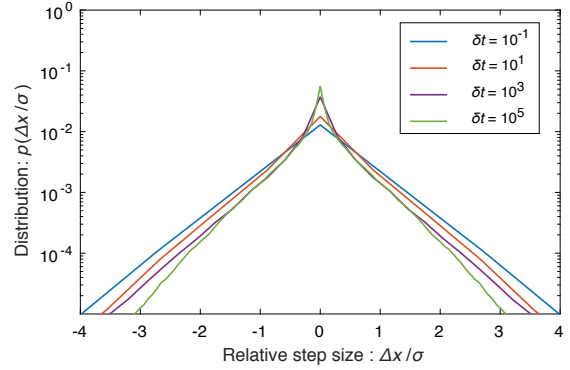

FIG. 7. **Barrier models in higher dimension.** Even though motion is diffusive at sufficiently long lag times, the crossover time between sub-diffusion and regular diffusion may be extremely long for strong disorder. The step-size distribution for very strong chi-squared disorder is shown above. The EVT-shape is preserved even in the longest lag times shown. (Simulations details in Sec. D 12.)

added dimensions is to renormalize (*i.e.* reduce) the effective one-dimensional barrier strength.

V. ANALYTIC RESULTS

The scale-invariant and generic properties of the motion observed in simulation suggest that a simple analytic framework many describe many characteristics of the motion. In this section, we will describe just such an approach that leverages results from extreme value theory.

A. Slowest-step model

The observation from simulation that the dynamics are limited by the slowest step, motivates a simple model for the step-size distribution roughly analogous to the Beer-Lambert law (*e.g.* [35]). Consider the probability of the particle escaping over n barriers with lattice spacing x_0: If the motion is limited by the largest barrier, we can approximate this probability as the probability that all n barriers are smaller than the largest barrier g that can be jumped in lag time δt:

$$\Pr\{\Delta x > n\,x_0\} \approx \Pr\{G_{1...n} < g\} = [F_G(g)]^n, \quad (9)$$

where the F_G is the CDF for barrier height G. If we substitute the relative displacement $|\Delta x| = n\,x_0$ for the barrier number n, the pdf for for displacement is a Laplace-like distribution:

$$\langle p(\Delta x) \rangle_G \approx \tfrac{1}{2}\lambda\, e^{-\lambda|\Delta x|}, \quad (10)$$

as observed, where the decay constant is specified by the CDF:
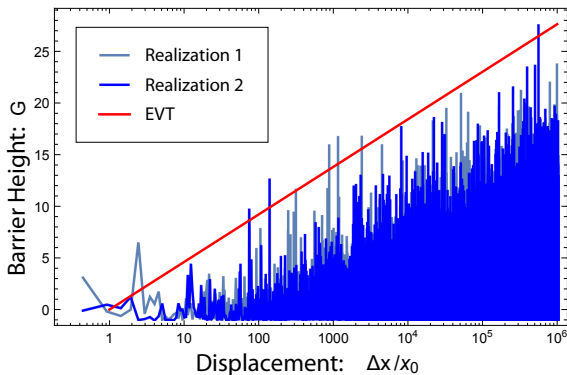
$$\lambda \equiv -x_0^{-1} \log F_G(g) \quad (11)$$

FIG. 8. **Limiting barrier height grows with displacement.** The barrier free energies for two realizations of G ($\beta = 1$) are plotted versus position on a linear-log plot. The EVT curve represents the extreme value prediction for the height of the maximum barrier as a function of displacement ($\Delta x/x_0$).

where x_0 is the lattice size and step-size variance:

$$\left\langle \Delta x^2 \right\rangle_G = \lambda^{-2} = [x_0 / \log F_G(g)]^2. \tag{12}$$

A more rigorous derivation and an exact expression for Eqn. 10 are given in the Appendix. (See Eqn. A19.) The slowest-step model can therefore be understood to imply the universal Laplace-like shape of the step-size distribution function. (See Fig. 8.) The Laplace-like step-size distribution had previously been proposed in the barrier model, but on a purely numerical basis [36].

The slowest-step model also explains strong-disorded-like behavior of normally distributed barriers (weak disorder) at short lag times. In this case, the disorder does not satisfy the strong disorder condition and therefore the step-size distribution is Gaussian and MSD is diffusive in the long time limit. However, for large variance, the step-size distribution is Laplace distributed and the MSD is sub-diffusive for intermediate times, as was previously reported [37]. (See Fig. 4C.) This phenomenology arises since the motion is limited by the slowest step on short times, but not long times.

B. Extreme value theory

Does the slowest-step model also give rise to a scale-independent MSD? The fact that the behavior is dominated by the largest barrier suggests the use of Extreme Value Theory (EVT) [5, 6]. In loose analogy to the central limit theorem, the Fisher-Tippett-Gnedenko theorem states that the CDF for the maximum $G_{(n)}$ of n independent and identically distributed random variables G in the large n limits takes the form of the generalized-extreme-value distribution:

$$F(g; \xi, \sigma, \mu) = \begin{cases} \exp[-(1 + \xi s)^{-1/\xi}] & \xi \neq 0 \\ \exp[-\exp(-s)] & \xi = 0 \end{cases}, \tag{13}$$

if the limit exists, where $s \equiv (g - \mu)/\sigma$, which depends only on three parameters: a location μ, scale σ and shape ξ [5, 6]. To exploit the EVT result, we coarse grain the system. We group adjacent lattice sites to generate a coarse-grained lattice: $x_0 \rightarrow x_0' = \Lambda x_0$. We will assume that in the coarse-grained system: (i) the motion is still limited by largest barrier and (ii) the dilation Λ is large enough such that the Generalized-extreme-value distribution (Eqn. 13) can be substituted for $F_{G'}$ in Eqn. 12. Finally, the limiting barrier height g scales with lag time δt:

$$g \approx \log \delta t/t_0' + \mu, \tag{14}$$

where t_0' is a constant time scale that absorbs the location parameter μ and fundamental relaxation time t_0. Combing this with Eqns. 13 and 12 gives an expression for the E-MSD:

$$\left\langle \Delta x^2 \right\rangle_G \approx 2\, x_0'^2 \begin{cases} [1 + (\xi/\sigma) \log \delta t/t_0']^{2/\xi} & \xi \neq 0 \\ (\delta t/t_0')^{2/\sigma} & \xi = 0 \end{cases}, \tag{15}$$

where ξ is the shape parameter and σ is the scale parameter of the generalized extreme value distribution.

We now consider three conditions on the shape parameter: $\xi > 0$, $\xi < 0$ and $\xi \approx 0$. (i) If $\xi < 0$, the distribution of G falls into the basin of attraction of the (reversed) Weibull distribution. In this case G is bounded from above and therefore the strong disorder assumption (Eqn. 2) is violated and the motion becomes diffusive in the long lag time limit. (ii) If $\xi > 0$, the limiting distribution is Fréchet (*e.g.* the distribution of G has power-law tails) and the MSD grows more slowly than a power-law. In this case, the effective MSD scaling exponent decreases with time. (iii) Finally, for disorder where the limiting distribution is Gumbel-like ($\xi \approx 0$), the MSD is scale-invariant with an MSD scaling parameter:

$$\alpha = 2/\sigma, \tag{16}$$

related to the EVT scale parameter σ. In this case, the E-MSD *is* scale invariant:

$$\left\langle \Delta x^2 \right\rangle_G \approx 2D\, \delta t^{2/\sigma}, \tag{17}$$

and the lattice spacing x_0' and time scale t_0' are absorbed into the generalized diffusion coefficient D in the MSD formula. In the special case that the disorder is modeled by a scaled chi-squared, $\alpha = \beta^{-1}$ as was observed empirically in simulation. (See the Appendix Sec. A3. An analogous limiting expression can be derived for the MSD using other methods [28].)

In summary, a quenched barrier model does generically result in a scale-invariant MSD, provided that the distribution of barrier free energies is strongly disordered (but without power-law tails). This analysis reveals that the EVT scale-parameter for the distribution of barrier free energies determines the MSD scaling exponent (Eqn. 16).

VI. DISCUSSION

The observed particle motion is scale invariant from the perspective of three metrics of the dynamics: (i) mean-squared-displacement analysis (MSD), (ii) the step-size distribution and (iii) the velocity autocorrelation function [18]. We have demonstrated that all three of these properties arise genericly in the context of the quenched barrier model in the strong disorder limit. In particular, the anti-correlation of successive steps is a key signature of both the barrier model as well as the observed data. For instance, the competing trap model is both sub-diffusive and has a Laplace-like step-size distribution (in the strong-disorder limit), but shows no anti-correlation in successive steps (Fig. 3). Although we previously modeled this anti-correlation empirically using a fBm mechanism [4], this phenomenology is an emergent feature of barrier models. In summary, although our previous work demonstrated that most of the observed phenomenology could be fit to a complex chimera of the fBm and Exp-D models, this observed phenomenology arises genericly in the context of barrier models. Furthermore, we tested whether the motion was consistent with a quenched diffusion coefficient combined with gaussian distributed steps, as predicted by the fBm-Exp-D model. Even at the single trajectory level, the step size distribution was better modeled by a Laplace distribution, as predicted by the barrier model (Sec. IV E).

We have made a number of formal assumptions in our model: (i) We first assumed that the free energy landscape is quenched, or static in time. From a practical perspective, it is necessary only that the dynamics of the quenched disorder is slow compared to the observed dynamics. If the barriers transition from quenched (static) to annealed (dynamic) on a short time scale, the particle motion transitions back to diffusive on longer timescales (*e.g.* [23]) and the velocity autocorrelation function would be zero. (ii) We also assume a strong-disorder limit in which the quenched-disorder-averaged hop time diverges. This is a convenient formal statistical assumption which can be violated without significant changes in the predictions of the model. The relevant physical assumption is that dynamics is limited by the slowest step, as is the case for normally distributed barriers with a short lag-time (Fig. 4C). (iii) The most consequential assumption is the effective one-dimensional motion. One-dimensional barriers are interpreted as effective barrier heights between positions along the long axis of the cell. The ability of the particles to take circuitous routes in higher dimension will always result in diffusive motion in the asymptotic large-time limit [19]. This crossover is observed in glasses ($\dim > 1$) [38] as well as simulations of the barrier model, where the long-time-limit dynamics transitions between sub-diffusive and diffusive. (Not shown.) Like-wise, the step-size distribution can be initially described by a Laplace-like distribution at short times before transitioning to a Gaus-

sian distribution at very long times (See Fig. 7). But these properties do not compromise the applicability of the barrier model in the context of our experiments. The finite length of the cell and cell cycle prevents an analogous long-time limit from being characterized experimentally. Furthermore, in the bacterial system, the confinement due to the cell membrane and nucleoid exclusion may act to make the dynamics effectively one-dimensional in the long-time limit [18].

A number of different physical mechanisms could generate the hypothesized *rough free-energy landscape*. A trap-like landscape is a natural model for particles that can bind with a distribution of binding free energies (*e.g.* transcription factors binding the chromosome). The trap model applies because the forward and backward jump rates are expected to be equal since hopping is limited by unbinding. On-the-other-hand, a barrier model would be a natural model for crowding and exclusion phenomena where entropic barriers frustrate the transition between *open* sites on the lattice (*e.g.* [35]). The forward and backward hop rates are expected to be distinct since these transitions hop over different configurations of crowders. (See Fig. 1.)

A. More realistic models

The proposed model is not intended to capture every aspect of the dynamics, but should be understood as an attempt to study a minimal model with the characteristics of the observed dynamics. For instance, the exclusion of particles from the nucleoid results in biases in the motion on long time-scales, which we have already characterized in some detail [18]. Furthermore, in many analogous tracking experiments, there does appear to be some ergodicity breaking [39, 40]. This phenomenology is naturally present in the models we have discussed by introducing traps and barriers. In many systems there may also be a significant degree of quenched disorder in the diffusion coefficient itself, consistent with our statistical analysis in Sec. IV E.

B. Barrier versus fBm models

The barrier model shares many phenomenological features with fBm and therefore it is natural to ask whether the barrier model is one specific realization of a more general fBm class of models. Barrier and fBm models are distinct. (*E.g.* fBm have Gaussian step-size distributions.) Another key distinction is their motivation. Barrier models are easily motivated by the underlying physics and there are no hidden states or variables since the memory of the system is encoded in the particle position. In contrast, fBm models are essentially phenomenological in nature [20, 41], although they can be justified in some cases (*e.g.* [42]). Therefore the barrier model provides a simple, but yet non-canonical, mecha-

nism for the emergence of the macroscopic phenomenon of velocity anti-correlation.

C. Strong disorder is generic in biology

The EVT mechanism may predict emergent scale-invariant behavior in other systems since strong disorder appears to be ubiquitous in biology. For instance, the motion of lipids and proteins in the membrane appear to show a barrier-hopping like phenomenology in some contexts. Lipids and membrane proteins appear to undergo relatively rapid motion in small confined membrane domains, then exhibit a slower hopping behavior between neighboring domains [43–45], which have been described by fence models [34]. If the interdomain hopping rate is strongly disordered, we would expect to see scale-invariant behavior due to an EVT mechanism. (Strong quenched disorder in the hopping rates is the essential assumption here since, in some simple simulated lipid systems, the dynamics appears to show relatively small deviations from diffusion [46, 47].) Another interesting potential application is chemical kinetics. In metabolism, reactions are often limited by the slowest step. If we treat these effective reaction rates as random variables, EVT might be used to predict the scaling of average reaction rate with reactant number. In the context of evolution, EVT has already been applied to describe fitness and beneficial mutations [9–11]. The framework may also have interesting applications beyond dynamics as well. For instance, high-resolution characterizations of DNA flexibility have previously re-ported bending probabilities with Laplace-like distributions suggesting that similar arguments may apply in mechanical contexts as well when studying the flexibility of DNA molecules with sequence dependent flexibility [48].

D. Conclusion

We have demonstrated that diffusion on a quenched rough free-energy landscape with strongly disordered barriers naturally gives rise to motion with the same scale-invariant dynamics observed for large complexes in the bacterial cytoplasm. In the strong disorder limit, this barrier model generically predicts all three observed scale-invariant phenomena: (i) MSD, (ii) relative step-size distribution and (iii) the velocity autocorrelation function as well as making other non-trivial predictions about the dynamics. We explain the emergent scale-invariant properties of model using an Extreme Value Theory framework. We expect this approach will be applicable to describing dynamics in many other biological systems.

Appendix A: Analysis

1. Model selection by information-based inference

a. Information-based model selection

Let the candidate probability distribution function be $q(X|\theta)$ where X are the observations and $\theta \in \Theta$ are the parameters. (For simplicity, we will consider only models where the steps are independent and identically distributed over a trajectory.) The Shannon information is defined:

$$h(X|\theta) \equiv -\log q(X|\theta). \tag{A1}$$

The maximum likelihood (minimum information) estimate for the parameters are defined:

$$\hat{\theta}_X \equiv \arg\min_\theta h(X|\theta), \tag{A2}$$

and the minimum information is $h(X|\hat{\theta}_X)$. The unbiased estimator of the information for a second data set (of the same sample size and structure as X), generated by the same stochastic process and encoded by parameters $\hat{\theta}_X$ is the Akaike Information Criterion (AIC) [31, 32]:

$$\text{AIC}(X) = h(X|\hat{\theta}_X) + K \quad \text{(nats)}, \tag{A3}$$

where K is the complexity which is equal to the model dimension ($K = \dim \Theta$) for a regular statistical model in the large sample size limit [31, 32]. The model with the smallest AIC value is selected. (See the statistical weight,

defined below.) The complexity corrects for the overfitting phenomenon and facilitates the direct comparison of models of different model dimension. AIC was originally defined in information units of demi-nats instead of nats (base-e). The historical definition therefore contains an extra factor of two multiplying the RHS of Eqn. A3 [31, 32]. The Akaike weight (relative statistical weight) for model i is:

$$w_i \propto e^{-\text{AIC}_i}. \tag{A4}$$

The information-based approach is particularly powerful in the context of selecting between multiple non-nested models [31, 32].

b. Empirical expectations

Let Δx_{iI} be the ith step in the Ith trajectory, the number of steps in the Ith trajectory be n_I, the number of trajectories be N and the total number of steps in all trajectories be n_T. We define empirical expectation of function f over trajectory I:

$$\overline{f(\Delta x_I)} \equiv n_I^{-1} \sum_{i=1}^{n_i} f(\Delta x_{iI}), \tag{A5}$$

and over all trajectories:

$$\overline{f(\Delta x)} \equiv n_\text{T}^{-1} \sum_{I=1}^{N} n_I \overline{f(\Delta x_I)}. \tag{A6}$$

c. Gaussian distribution with trajectory-specific variance

For the Gaussian distribution with trajectory-specific variance σ_I^2, the total information for trajectory I is:

$$h(\Delta x_I | \sigma_I^2) = \frac{n_I}{2} \left[\log 2\pi\sigma_I^2 + \frac{\overline{\Delta x_I^2}}{\sigma_I^2} \right]. \tag{A7}$$

It is straight forward to show that $\hat{\sigma}_I^2 \equiv \overline{\Delta x_I^2}$ by minimizing h. AIC for trajectory I is:

$$\text{AIC}(\Delta x_I) = \frac{n_I}{2} \left[\log 2\pi\overline{\Delta x_I^2} + 1 \right] + 1, \tag{A8}$$

where $K = 1$ since there is one unknown parameter (σ_I^2). AIC for all N trajectories is computed by summing over the individual trajectories:

$$\text{AIC}(\Delta x) = \sum_{I=1}^{N} \frac{n_I}{2} \left[\log 2\pi\overline{\Delta x_I^2} + 1 \right] + N. \tag{A9}$$

d. Laplace distribution with trajectory-specific decay constants

For the Laplace distribution with trajectory-specific decay constant λ_I, the information for trajectory I is:

$$h(\Delta x_I | \lambda_I) = n_I \left[\log \frac{2}{\lambda_I} + \lambda \overline{|\Delta x_I|} \right]. \tag{A10}$$

It is straight forward to show that $\hat{\lambda}_I \equiv \overline{|\Delta x_I|}^{-1}$ by minimizing h. AIC for trajectory I is:

$$\text{AIC}(\Delta x_I) = n_I \left[\log 2\overline{|\Delta x_I|} + 1 \right] + 1. \tag{A11}$$

where $K = 1$ since there is one unknown parameter (λ_I). AIC for all N trajectories is computed by summing over the individual trajectories:

$$\text{AIC}(\Delta x) = \sum_{I=1}^{N} n_I \left[\log 2\overline{|\Delta x_I|} + 1 \right] + N. \tag{A12}$$

e. Laplace distribution with one decay constants

For the Laplace distribution with a single λ the computation is analogous to that shown above:

$$\mathrm{AIC}(\Delta x) = n_{\mathrm{T}} \left[\log 2\overline{|\Delta x|} + 1 \right] + 1, \tag{A13}$$

where $K = 1$ since there is one unknown parameter λ.

f. Comments

Note that since Δx has units, AIC has a unit-dependent offset which drops out when difference of AIC are computed. A convenient check of the information-based statistical approach is to compute $\Delta\mathrm{AIC}$ for simulated Gaussian and Laplace distributed data with the same structure as the observed data. For Laplace distributed data, $\Delta\mathrm{AIC} = 1.5 \times 10^4$ nats, strongly favoring the Laplace-distributed model. For Gaussian distributed data, $\Delta\mathrm{AIC} = -1.3 \times 10^4$ nats, strongly favoring the Gaussian-distributed model, as expected.

2. Exact treatment of slowest step model

We shall assume that the particle begins at lattice site $i = 0$ and that over lag time t the particle equilibrates over the lattice sites between the trapping barriers at positions $-J$ and K respectively. Let ϵ be the probability that a given barrier is too large to hop. The probability for the limiting barrier positions are:

$$p_J(j - \tfrac{1}{2}) = \epsilon(1-\epsilon)^{j-1}, \tag{A14}$$

$$p_K(k - \tfrac{1}{2}) = \epsilon(1-\epsilon)^{k-1}, \tag{A15}$$

respectively with $\Delta L(J, K) = J + K$ accessible lattice sites, where j and k are natural numbers and the barriers are located at half-integer positions. The equilibration assumption implies that the probability of occupancy of a site between the limiting barriers is:

$$p(i| - J, K) = \Delta L^{-1}. \tag{A16}$$

We then compute the marginal likelihood $p(i)$ by marginalizing over J and K using probabilities in Eqns. A14 and A15:

$$p(i) = \sum_{k=1, j=|i|+1}^{\infty} \frac{p_J(j - \tfrac{1}{2}) p_K(k - \tfrac{1}{2})}{\Delta L(j - \tfrac{1}{2}, k - \tfrac{1}{2})}, \tag{A17}$$

$$= \sum_{k=1, j=|i|+1}^{\infty} \frac{\epsilon^2 (1-\epsilon)^{j+k-2}}{k + j - 1}, \tag{A18}$$

$$= e^{-\lambda'|i|} \cdot \sum_{k=1, j=1}^{\infty} \frac{\epsilon^2 (1-\epsilon)^{j+k-2}}{|i| + k + j - 1}, \tag{A19}$$

where $\lambda' \equiv -\log(1 - \epsilon)$. The dominant Laplace-like scaling with lattice-site displacement i is clear from the first factor in Eqn. A19. The second factor has a weaker dependence on i. By *Laplace-like* distribution, we mean the the log probability has the following scaling in the lattice displacement i:

$$\log p(i) = -\lambda'|i| + \mathbb{O}(\log|i|), \tag{A20}$$

where $\mathbb{O}$ denotes the order of scaling.

3. Gumbel parameters for chi-squared distribution

In this section, we compute the scale and location parameters for the chi-squared distribution. The cumulative distribution for a chi-squared is:

$$\mathrm{Pr}_{\chi_1^2}\{X > x\} = F_{\chi_1^2}(x) = \Gamma^{-1}(\tfrac{1}{2}) \, \gamma(\tfrac{1}{2}, \tfrac{x}{2}), \tag{A21}$$

where Γ is the gamma function and γ is the lower incomplete gamma function $\gamma(s, z)$. To find the Gumbel location and scale parameters, we solve the following approximate equality for large x and N:

$$\exp\left[-N\exp\left(-\frac{x-\mu}{\sigma}\right)\right] \approx -\log N + \frac{x}{2} + \log\Gamma(s) - (s-1)\log\log N + ... \tag{A22}$$

Matching up terms on the right and left, we have :

$$\sigma_N \equiv 2, \tag{A23}$$

$$\mu_N \equiv 2\log N - \log\log N - 2\log\Gamma(\tfrac{1}{2}) + ... \tag{A24}$$

We now convert to the free-energy random variable $G \equiv \beta X$, which β is the variance. The re-parameterization results in

$$\delta g \equiv 2\beta, \tag{A25}$$

$$g_0 \equiv 2\beta\left[-\tfrac{1}{2}\log\log N - \log\Gamma(\tfrac{1}{2})\right] + ... \tag{A26}$$

which leads to a simple result for the scaling exponent: $\alpha = \beta^{-1}$, *i.e.* the inverse of the disorder strength for strong disorder.

Appendix B: Simulations

For all simulations, we begin with the initial condition that all sites on the lattice have equal initial probability.

1. Master Equation

The master equation describing the lattice hopping model is:

$$\dot{p}_i = k_{i-1/2}p_{i-1} + k_{i+1/2}p_{i+1} - (k_{i-1/2} + k_{i+1/2})p_i, \tag{B1}$$

where p_i is the probability distribution of the particles at the occupancy state i and $k_{i+1/2}$ is the hopping rate through the transition state $i + 1/2$. We use periodic boundary conditions at the end points. To solve the master equation for individual realizations of the quenched disorder, we use the built-in matrix exponentiation in MATLAB (expm):

$$\boldsymbol{p}(t; \{G\}) = e^{\boldsymbol{K}(\{G\})t}\boldsymbol{p}(0), \tag{B2}$$

where $\boldsymbol{K}$ is the rate matrix given free energies G.

2. Gillespie Simulation

For the simulations of the trajectories we use a stochastic Gillespie simulation [49, 50]. To obtain the next occupancy site at regular time intervals, we use a modification of the Gillespie simulation [51]. In short, for each time step $\Delta t'$ we define the total hopping rate k_{tot}, equal to the sum of the hopping rates to every neighboring lattice site. The probability that the particle has transitioned to a neighboring state during the time step $\Delta t'$ is dictated by CDF $P(\Delta t') = 1 - \exp(-k_{\text{tot}}\Delta t')$. The transition occurs if a random number r_1, uniformly distributed between 0 to 1, is smaller than the CDF $P(\Delta t')$. If the transition is to take place, the new occupancy state is found using a second random number r_2, evenly distributed from 0 to 1, and the cumulative probability distribution of the adjacent hopping rates. To allow for additional transitions between t_{new} and $t_{\text{current}} + \Delta t'$ we repeat the same procedure with a shortened time step:

$$\delta t' = t_{\text{current}} + \Delta t' - t_{\text{new}}. \tag{B3}$$

The process is repeated until no transition takes place.

Appendix C: Free energy probability distributions

For convenience, we include explicit definition of the probability distributions which were used in the article for the free energy barriers. In each case, the disorder strength β of the free energies was defined by multiply the random variable X by the disorder strength:

$$G \equiv \beta X. \tag{C1}$$

The **chi-squared distribution** is defined by the PDF:

$$p(x; k) = \frac{1}{2^{k/2}\Gamma(k/2)} \, x^{k/2-1} \, \mathrm{e}^{-x/2}, \tag{C2}$$

for dimension k and x has support $x \in [0, \infty)$. In our simulations, we used dimension $k = 1$. The **normal distribution** is defined:

$$p(x; \mu, \sigma) = \frac{1}{\sqrt{2\pi\sigma^2}} \, \mathrm{e}^{-(x-\mu)^2/2\sigma^2}, \tag{C3}$$

for mean μ and standard deviation σ and x has support $x \in (\infty, \infty)$. In our simulations we used $\mu = 0$ and $\sigma = 1$. The **exponential distribution** is defined:

$$p(x; k) = k \, \mathrm{e}^{-kx}, \tag{C4}$$

where k is the rate and x has support $x \in [0, \infty)$. In our simulations, we used rate $k = 1$. The **Gumbel distribution** is defined by the CDF:

$$P(x; \mu, \sigma) = \exp[-\exp[-(x - \mu)/\sigma]], \tag{C5}$$

where μ is the position and σ is the scale parameter respectively and x has support $x \in (\infty, \infty)$. For our simulations, we used $\mu = 0$ and $\sigma = 1$.

In each case we use the CDF method for generating random variables: We first generate uniformly distributed random variable (Y) with support on the interval $Y \in [0, 1]$ and then use the inverse CDF to generate X:

$$X_i \equiv P^{-1}(Y_i). \tag{C6}$$

Appendix D: Plot simulation details

1. Details for Fig. 1D

Trap model: Chi-squared distributed traps: $G_i = -\beta X$ and $G_{i+\frac{1}{2}} = 0$ with $\beta = 1.5$ and $t_0 = 1$ (Eqn. 1) to define the rates. Trajectories were generated using a Gillespie simulation (Sec. B 2). The time interval shown was $T = 1000 \, t_0$.
Barrier model: Chi-squared distributed barriers: $G_i = 0$ and $G_{i+\frac{1}{2}} = \beta X$ with $\beta = 1.5$ and $t_0 = 1$ (Eqn. 1) to define the rates. Trajectories were generated using a Gillespie simulation (Sec. B 2). The time interval shown was $T = 1000 \, t_0$.

2. Details for Fig. 2A

All model curves: Barrier model with chi-squared distributed barriers: $G_i = 0$ and $G_{i+\frac{1}{2}} = \beta X$ and $t_0 = 1$ (Eqn. 1) to define the rates. MSDs were computed using the master equation (Sec. B 1). Simulations were performed on a 10^5 site-lattice with periodic boundary conditions. $N = 50$ realizations were averaged.

3. Details for Fig. 2B

Same as above. Scaling exponent α was estimated by fitting on the interval $\delta t/t_0 \in [10^6, 10^8]$.

4. Details for Fig. 2C

Barrier model: Chi-squared distributed barriers: $G_i = 0$ and $G_{i+\frac{1}{2}} = \beta X$, $\beta = 1.5$ and $t_0 = 1$ (Eqn. 1) to define the rates. **Trap model:** Chi-squared distributed barriers: $G_i = 0$ and $G_{i+\frac{1}{2}} = \beta X$, $\beta = 1.5$ and $t_0 = 1$ (Eqn. 1) to define the rates. For the T-MSD: The total time interval averaged over was $T = 10^{10} t_0$. The initial conditions for both models was a uniform distribution over all lattice points.

5. Details for Fig. 3

Trap model: Chi-squared distributed traps: $G_i = -\beta X$ and $G_{i+\frac{1}{2}} = 0$ with $\beta = 1.5$ and $t_0 = 1$ (Eqn. 1) to define the rates. **Barrier model**: Chi-squared distributed barriers: $G_i = 0$ and $G_{i+\frac{1}{2}} = \beta X$ with $\beta = 1.5$ and $t_0 = 1$ (Eqn. 1) to define the rates. VACs/DACs were computed using the master equation (Sec. B 1). Simulations were performed on a 10^4 site-lattice with periodic boundary conditions.

6. Details for Fig. 4A

Barrier model: Chi-squared distributed barriers: $G_i = 0$ and $G_{i+\frac{1}{2}} = \beta X$ with $\beta = 5$ and $t_0 = 1$ (Eqn. 1) to define the rates. Relative step size distributions were computed using the master equation (Sec. B 1). $N = 50$ realizations were averaged. Simulations were performed on a 10^4 site-lattice with periodic boundary conditions.

7. Details for Fig. 4B

Barrier model: Chi-squared distributed barriers: $G_i = 0$ and $G_{i+\frac{1}{2}} = \beta X$ and $t_0 = 1$ (Eqn. 1) to define the rates. Relative step size distributions were computed using the master equation (Sec. B 1) for time interval $\delta t = 100 t_0$. $N = 50$ realizations were averaged. Simulations were performed on a 10^4 site-lattice with periodic boundary conditions.

8. Details for Fig. 4C

Barrier model: This disorder strengths and time interval were: $\beta = 5$ and $\delta t = 10^3 t_0$ for Chi-squared, Exponential and Gumbel, $\beta = 3.0$ and $t_0 = 0.1 t_0$ for short normal and $\beta = 0.3$ and $t_0 = 0.1 t_0$ for long normal. Relative step size distributions were computed using the master equation (Sec. B 1) for time interval $\delta t = 100 t_0$. $N = 50$ realizations were averaged. Simulations were performed on a 10^4 site-lattice with periodic boundary conditions.

9. Details for Fig. 5A

Barrier model: Chi-squared with disorder strengths and time interval: $\beta = 5$ and $\delta t = 10^3 t_0$. $N = 50$ realizations were averaged. Simulations were performed on a 10^4 site-lattice with periodic boundary conditions. Conditional step size distributions were computed using the master equation (Sec. B 1) **Trap model**: Chi-squared with disorder strengths and time interval: $\beta = 5$ and $\delta t = 10^3 t_0$. $N = 50$ realizations were averaged. Simulations were performed on a 10^4 site-lattice with periodic boundary conditions. Conditional step size distributions were computed using the master equation (Sec. B 1) **fBm model**: The built-in MATLAB function `wfbm` was used to generate fBM trajectories. To match the observed scaling exponent ($\alpha \approx 0.65$), we used a Hurst parameter $H = 0.32$. **fBm-Exp-D model**: Same as fBm, but the trajectories were scaled to generate an exponential distribution of diffusion coefficients on the interval $[0.005, 5.2]$. **Exp-D model**: Canonical diffusion with quenched diffusion coefficient. The diffusion coefficient was exponentially distributed on the interval $[0.005, 5.2]$. The time interval was $\delta t = t_0$. Conditional step size distributions were computed analytically at fixed D then weighted numerically over D. **Diffusion model**: Conditional step size distributions were computed analytically.

10. Details for Fig. 5B

Barrier model: Chi-squared with disorder strengths and time interval: $\beta = 5$ and $\delta t = 10^3 \, t_0$. $N = 50$ realizations were averaged. Simulations were performed on a 10^4 site-lattice with periodic boundary conditions. Conditional step size distributions were computed using the master equation (Sec. B 1). KDE: The kernel was normal with $\sigma = 0.2$.

11. Details for Fig. 6

Barrier model: Chi-squared with disorder strength $\beta = 5$. Simulations were performed on a 10^4 site-lattice with periodic boundary conditions. The Greens function was computed using the master equation (Sec. B 1).

12. Details for Fig. 7

Barrier model: Chi-squared with disorder strength $\beta = 18$ and $t_0 = 1$ in two dimensions. Simulations were performed on a $10^3 \times 10^3$ site-lattice with periodic boundary conditions. Trajectories were simulated using the Gillespie simulation method. (Sec. B 1). $N = 100$ realizations were averaged for 10^6 step trajectories.

———————————————————

[1] G. B. West, J. H. Brown, and B. J. Enquist, Science **276**, 122 (1997).
[2] M. Hegreness, N. Shoresh, D. Hartl, and R. Kishony, Science **311**, 1615 (2006).
[3] R. Milo and R. Phillips, *Cell Biology by the Numbers* (Garland Science, 2015).
[4] T. J. Lampo, S. Stylianidou, M. P. Backlund, P. A. Wiggins, and A. J. Spakowitz, Biophysical Journal (2017).
[5] S. Resnick, *Extreme values, regular variation, and point processes* (Springer-Verlag, 1987).
[6] M. Leadbetter, G. Lindgren, and H. Rootze, *Extremes and related properties of random sequences and processes.* (Springer-Verlag, 1983).
[7] J.-P. Bouchaud and M. Mézard, J. Phys. A: Math. Gen. **30**, 7997 (1997).
[8] B. Derrida, Physical Review B (1981).
[9] S. A. Frank, Journal of evolutionary biology **27**, 1172 (2014).
[10] H. A. Orr, Philosophical Transactions of the Royal Society of London B: Biological Sciences **365**, 1195 (2010).
[11] P. Joyce, D. R. Rokyta, C. J. Beisel, and H. A. Orr, Genetics **180**, 1627 (2008).
[12] M. Gherardi, F. Bassetti, and M. Cosentino Lagomarsino, Phys Rev E **93**, 042307 (2016).
[13] M. Weiss, H. Hashimoto, and T. Nilsson, Biophysical journal **84**, 4043 (2003).
[14] I. Golding and E. C. Cox, Proc Natl Acad Sci U S A **101**, 11310 (2004).
[15] I. Bronstein, Y. Israel, E. Kepten, S. Mai, Y. Shav-Tal, E. Barkai, and Y. Garini, Phys. Rev. Lett. **103**, 018102 (2009).
[16] S. C. Weber, A. J. Spakowitz, and J. A. Theriot, Phys. Rev. Lett. **104**, 238102 (2010).
[17] F. Höfling and T. Franosch, Reports on Progress in Physics **76**, 046602 (2013).
[18] S. Stylianidou, N. J. Kuwada, and P. A. Wiggins, Biophys J **107**, 2684 (2014).
[19] J.-P. Bouchaud and A. Georeges, Physics Reports **195**, 127 (1990).
[20] R. Metzler, J.-H. Jeon, A. G. Cherstvy, and E. Barkai, Physical Chemistry Chemical Physics **16**, 24128 (2014).
[21] P. Massignan, C. Manzo, J. Torreno-Pina, M. García-Parajo, M. Lewenstein, and G. Lapeyre Jr, Physical review letters **112**, 150603 (2014).
[22] C. Manzo, J. A. Torreno-Pina, P. Massignan, G. J. Lapeyre Jr, M. Lewenstein, and M. F. G. Parajo, Physical Review X **5**, 011021 (2015).
[23] B. Wang, J. Kuo, S. C. Bae, and S. Granick, Nature materials **11**, 481 (2012).
[24] S. Stylianidou, C. Brennan, S. B. Nissen, N. J. Kuwada, and P. A. Wiggins, Molecular Microbiology **102**, 690 (2016).
[25] S. B. Zimmerman and A. P. Minton, Annu Rev Biophys Biomol Struct **22**, 27 (1993).
[26] B. R. Parry, I. V. Surovtsev, M. T. Cabeen, C. S. O'Hern, E. R. Dufresne, and C. Jacobs-Wagner, Cell **156**, 183 (2014).
[27] N. J. Kuwada, B. Traxler, and P. A. Wiggins, Mol Microbiol **95**, 64 (2015).
[28] S. Alexander, J. Bernasconi, W. Schneider, and R. Orbach, Reviews of Modern Physics **53**, 175 (1981).
[29] J.-P. Bouchaud, A. Georges, and Le Doussal, Journal de physique **48**, 1855 (1987).
[30] R. Zwanzig, Proc Natl Acad Sci U S A **85**, 2029 (1998).
[31] H. Akaike, in *2nd International Symposium of Information Theory.*, edited by P. B. N. and E. Csaki (Akademiai Kiado, Budapest., 1973) pp. 267–281.
[32] K. P. Burnham and D. R. Anderson, *Model selection and multimodel inference.*, 2nd ed. (Springer-Verlag New York, Inc., 1998).
[33] S. Alexander, Physical Review B **23**, 2951 (1981).

[34] A. Kusumi, C. Nakada, K. Ritchie, K. Murase, K. Suzuki, H. Murakoshi, R. S. Kasai, J. Kondo, and T. Fujiwara, Annu Rev Biophys Biomol Struct **34**, 351 (2005).

[35] R. Phillips, J. Kondev, and J. Theriot, *Physical Biology of the Cell* (Garland Science, 2008).

[36] J. Bernasconi, W. Schneider, and W. Wyss, Zeitschrift für Physik B Condensed Matter **37**, 175 (1980).

[37] I. Goychuk and V. O. Kharchenko, Phys Rev Lett **113**, 100601 (2014).

[38] E. R. Weeks, J. C. Crocker, A. C. Levitt, A. Schofield, and D. A. Weitz, Science **287**, 627 (2000).

[39] J.-H. Jeon, V. Tejedor, S. Burov, E. Barkai, C. Selhuber-Unkel, K. Berg-Sørensen, L. Oddershede, and R. Metzler, Phys Rev Lett **106**, 048103 (2011).

[40] S. M. A. Tabei, S. Burov, H. Y. Kim, A. Kuznetsov, T. Huynh, J. Jureller, L. H. Philipson, A. R. Dinner, and N. F. Scherer, Proc Natl Acad Sci U S A **110**, 4911 (2013).

[41] B. B. Mandelbrot and J. W. van Ness, SIAM Rev **10** (1968).

[42] L. Lizana, T. Ambjörnsson, A. Taloni, E. Barkai, and M. A. Lomholt, Phys Rev E Stat Nonlin Soft Matter Phys **81**, 051118 (2010).

[43] H. Feinberg, D. A. Mitchell, K. Drickamer, and W. I. Weis, Science **294**, 2163 (2001).

[44] J.-B. Masson, P. Dionne, C. Salvatico, M. Renner, C. G. Specht, A. Triller, and M. Dahan, Biophysical journal **106**, 74 (2014).

[45] A. Sergé, N. Bertaux, H. Rigneault, and D. Marguet, Nature methods **5**, 687 (2008).

[46] J.-H. Jeon, H. M.-S. Monne, M. Javanainen, and R. Metzler, Phys Rev Lett **109**, 188103 (2012).

[47] J.-H. Jeon, M. Javanainen, H. Martinez-Seara, R. Metzler, and I. Vattulainen, Physical Review X **6**, 021006 (2016).

[48] P. A. Wiggins, T. van der Heijden, F. Moreno-Herrero, A. Spakowitz, R. Phillips, J. Widom, C. Dekker, and P. C. Nelson, Nat Nanotechnol **1**, 137 (2006).

[49] D. T. Gillespie, The journal of physical chemistry **81**, 2340 (1977).

[50] D. T. Gillespie, Annu. Rev. Phys. Chem. **58**, 35 (2007).

[51] S. Mehraeen, N. Cordella, J. S. Yoo, and A. J. Spakowitz, Soft Matter **7**, 8789 (2011).